Journal of Luminescence 145 (2014) 425–429

Contents lists available at ScienceDirect

Journal of Luminescence

journal homepage: www.elsevier.com/locate/jlumin

Energy band structure investigation of blue and green light emitting Mg doped SnO_2 nanostructures synthesized by combustion method

P.S. Shajira, M. Junaid Bushiri*, Bini B. Nair, V. Ganeshchandra Prabhu

Department of Physics, Cochin University of Science and Technology, Kochi 682022, Kerala, India

ARTICLE INFO

Article history:
Received 21 May 2013
Received in revised form
25 July 2013
Accepted 31 July 2013
Available online 14 August 2013

Keywords:
SnO_2
Combustion
Photoluminescence
Defect
Band structure

ABSTRACT

Tin oxide (SnO_2) and Mg doped (2, 4, 6, and 8 wt%) SnO_2 nanoparticles were synthesized by the self-propagating solution combustion synthesis using citric acid as fuel. The characterization of samples was done by X-ray diffraction spectroscopy (XRD), transmission electron microscopy (TEM), UV–visible spectroscopy, SAED and photoluminescence (PL). XRD pattern and TEM studies show that the synthesized particles are of average size 30 nm and they are in tetragonal rutile structure of SnO_2. Combined blue and green emission is seen in 4 wt% Mg doped SnO_2 and intensity of blue band is increased with respect to increase in Mg dopant concentration which is attributed to increase in population of oxygen vacancies. The PL emission in blue and green region is due to the doubly charged state (V_o^{2+}) of oxygen and tin interstitial defects respectively and is explained with an energy band diagram.

1. Introduction

Tin oxide (SnO_2) is a wide band gap n-type semiconducting material (E_g=3.6 eV at 300 K) which has good electric conductivity and optical transparency [1]. This property makes the material for applications in solar cells, flat panel displays, catalysts, gas sensors and optoelectronic devices like light emitting diodes [2–6]. Recently, more interest is focused on white light emission using non-toxic and stable materials. Blue and green emission sources can be effectively used for electron injection process in hetero-junction LEDs in order to generate white light [7]. The bulk SnO_2 is not luminescent, however nanosized SnO_2 exhibits a strong luminescence, contributed to surface defects, tin interstitials, dangling bonds or oxygen vacancies in the near surface region [8–11]. It is previously reported that a broad symmetric band centered around 560 nm in SnO_2 nanowires are attributed to structural defects [12]. However fish bone like SnO_2 nanostructures gives PL peak at 597 nm and beak like nanorods exhibit strong emission peaks at 602 nm due to oxygen vacancies [13,14]. An emission at 400 nm was observed in 2.8 nm sized SnO_2 [15]. SnO_2 nanoparticle has shown emission at 397 nm resulted from the oxygen vacancy [16]. Depending on the preparation condition, the types and numbers of defects, morphology and light emitting properties may vary.The structural and physical properties of SnO_2 also depend on the preparation method. There are several methods like spray pyrolysis, hydrothermal method, chemical vapor deposition, thermal evaporation, sol–gel method and chemical route are being used for the preparation of transition metal doped SnO_2 nanomaterials [17–22]. Apart from these methods, simple and cost effective solution combustion method is also being used [23].

In the present study, SnO_2 nanopowders as well as Mg doped SnO_2 were synthesized using solution combustion method using citric acid as fuel. The photoluminescence characteristics of SnO_2 and Mg doped SnO_2 are investigated. The contribution of Mg^{2+} ion on the photoluminescence nature of SnO_2 is studied in detail.

2. Experimental

2.1. Material preparation

Tin oxide nanopowder was synthesized by the self-propagating solution combustion synthesis. Stochiometric amounts of oxidizer (Tin chloride, $SnCl_4$, 3 g) and fuel (Citric acid, $C_6H_8O_7 \cdot H_2O$, 5.579 g), calculated based on the oxidizing and reducing vacancies were dissolved in deionized distilled water. The concentration of Mg^{2+} ion was varied from 2 to 8 wt% with respect to tin ion by using $MgCl_2$ in the initial reactants for doping. 30 ml of HNO_3 is added to the mixed solution which is the optimized quantity in order to get high yield. The pH of the solution was adjusted to 7 by adding NH_4OH. The resultant clear solution was heated on a hot plate maintained at a temperature of 200 °C inside a combustion

* Corresponding author. Tel.: +91 9495348631.
E-mail address: junaidbushiri@gmail.com (M.J. Bushiri).

0022-2313/$ - see front matter © 2013 Elsevier B.V. All rights reserved.
http://dx.doi.org/10.1016/j.jlumin.2013.07.073

chamber. The solution get foamed up and ignited, forming a sponge-like mass.

2.2. Characterization

The samples were characterized by an X-ray diffractometer (Rigaku) using Cu-Kα radiation ($\lambda = 1.5414$ Å). TEM measurements were performed with JEOL JEM 2100 High Resolution Transmission Electron Microscope (HRTEM) operated at 200 keV. UV–visible reflectance measurements were carried out using a spectrophotometer (Jasco V 570) in the range between 190 and 800 nm. PL of the prepared samples was measured by a spectroflurometer (Flurolog-3) with excitation source of 325 nm.

3. Results and discussion

3.1. XRD analysis of as synthesized samples

The X- ray diffraction peaks of the samples are sharp indicating the highly crystalline nature of the particle (Fig. 1). Peaks corresponding to diffraction planes (110), (101), (200), (211), (220), (002), (221), (112), (301), (202) and (321) can be seen and are in agreement with the standard JCPDS values (File no. 41-1445). This observation indicates that the nanoparticles are in tetragonal rutile phase of SnO_2. The XRD pattern of Mg doped SnO_2 nanoparticles is almost similar to that of SnO_2 nanoparticles with slight variation in unit cell parameters which indicates the incorporation of Mg ions into SnO_2 host lattice (Table 1). The XRD pattern of Mg doped SnO_2 shows a shift towards lower angle, attributedto the stress introduced by the incorporation of Mg^{2+} ions in Sn^{4+} site.

Average grain size is calculated by using Scherrer's formula [24] which shows slight variation in grain size while doping with Mg under identical experimental conditions. The obtained values for SnO_2 and 2, 4, 6 and 8 wt% Mg doped SnO_2 are 31, 35, 29, 31, 33 nm respectively (Table 2).

The calculated lattice parameters viz. "*a*" is slightly increased and "*c*" is slightly decreased in Mg doped SnO_2 crystals as compared to that of SnO_2 (Table 1). This observation indicates that there is an increase in population of oxygen vacancies, vacancy clusters and local lattice disorders in Mg doped SnO_2 [25,26].

3.2. TEM analysis

Transmission electron microscopy (TEM) images (Fig. 2a) show that the particles are nearly spherical in shape but in agglomerated form. The size distribution in the material is not uniform. The diameter of the particles varies from 25 to 36 nm which is comparable with the results obtained from the XRD with slight variation. The difference in average grain size from XRD data thus may be due to the nonuniform size distribution. The high resolution TEM (Fig. 2b) shows that the obtained particles are highly crystalline and the lattice spacing between the two planes is 0.185 nm which corresponds to (211) plane of SnO_2 tetragonal rutile structure. The rings in the SAED pattern can be indexed to (110), (101), (200), (211) and (112) planes of SnO_2 rutile structure (JCPDS Card File no. 41-1445). These results are in agreement with the previously discussed XRD result.

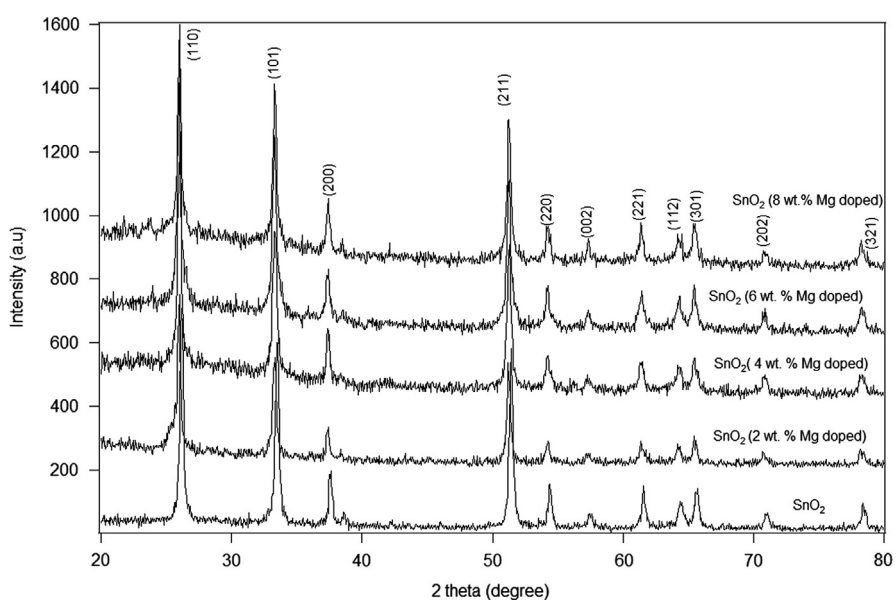

Fig. 1. XRD patterns of SnO_2 and Mg doped SnO_2 synthesized by the solution combustion method.

Table 1
Lattice parameters $\mathbf{a_{110}}$, $\mathbf{a_{200}}$,$\mathbf{c_{101-110}}$ and $\mathbf{c_{101-200}}$ calculated with XRD peaks corresponds to (100), (110) and (200) planes.

Sample	a_{110}	a_{200}	$\Delta a = a_{110} - a_{200}$	$c_{101-110}$	$c_{101-200}$	$\Delta c = c_{101-110} - c_{101-200}$
SnO_2	4.811	4.785	0.026	3.218	3.226	−0.008
2 wt% Mg doped SnO_2	4.851	4.811	0.04	3.234	3.246	−0.012
4 wt% Mg doped SnO_2	4.844	4.808	0.036	3.232	3.243	−0.011
6 wt% Mg doped SnO_2	4.847	4.810	0.037	3.235	3.246	−0.011
8 wt% Mg doped SnO_2	4.845	4.808	0.037	3.232	3.244	−0.012

3.3. Optical reflectance study

UV–visible diffuse reflectance spectra (DRS) measured in the wavelength range 190–800 nm at room temperature are as shown in Fig. 3. Reflection is maximum at visible region and shows a sharp reflection edge at wavelength 310–350 nm. The optical band gap of the samples was calculated from a plot of $\{(k/s)^{*}h\nu\}^2$ vs. $h\nu$ where "*k*" and "*s*" denote absorption and scattering coefficients, and $h\nu$ is photon energy [27]. Minor modifications in band gap while doping with Mg is observed (Fig. 4). The obtained values of band gaps are 3.63, 3.82, 3.75, 3.73 and 3.67 eV respectively for SnO_2 and Mg doped SnO_2 with doping concentrations 2, 4, 6 and 8 wt% (Table 2). In 2 wt% Mg doped SnO_2 the band gap becomes wider as a result of doping and band gap values found to be decreases with increase in Mg dopant concentration. Band gap likely to increase while doping with donors and decrease on acceptor doping in oxide semiconductors [28,29]. Mg substitution in Sn site may create two holes because of lower valancy of Mg^{2+} ion as compared to Sn^{4+} ion. Creation of additional holes likely to

Table 2
Grain size and optical properties of SnO_2 and Mg doped SnO_2 synthesized by the solution combustion method.

Sample	Average grain size (nm)	Band gap (eV)	PL peak intensity ratio (I_b/I_g)
SnO_2	31	3.63	0.18
2 wt% Mg doped SnO_2	35	3.82	0.8, 0.7
4 wt% Mg doped SnO_2	29	3.75	1.05
6 wt% Mg doped SnO_2	31	3.73	1.28
8 wt% Mg doped SnO_2	33	3.67	2.56

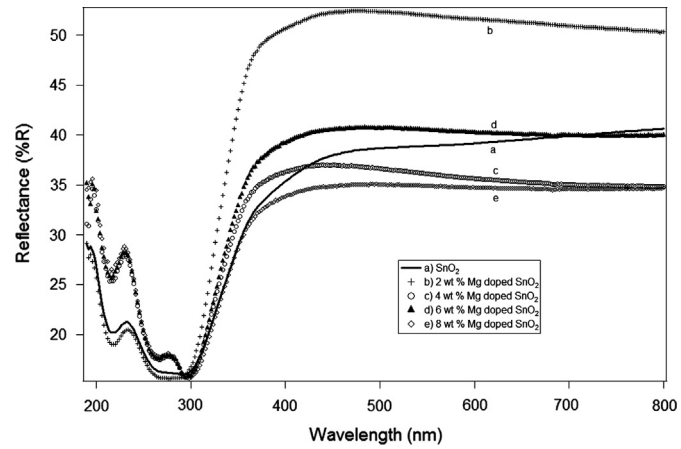

Fig. 3. Reflectance spectra of SnO_2 and Mg doped SnO_2 synthesized by the solution combustion method.

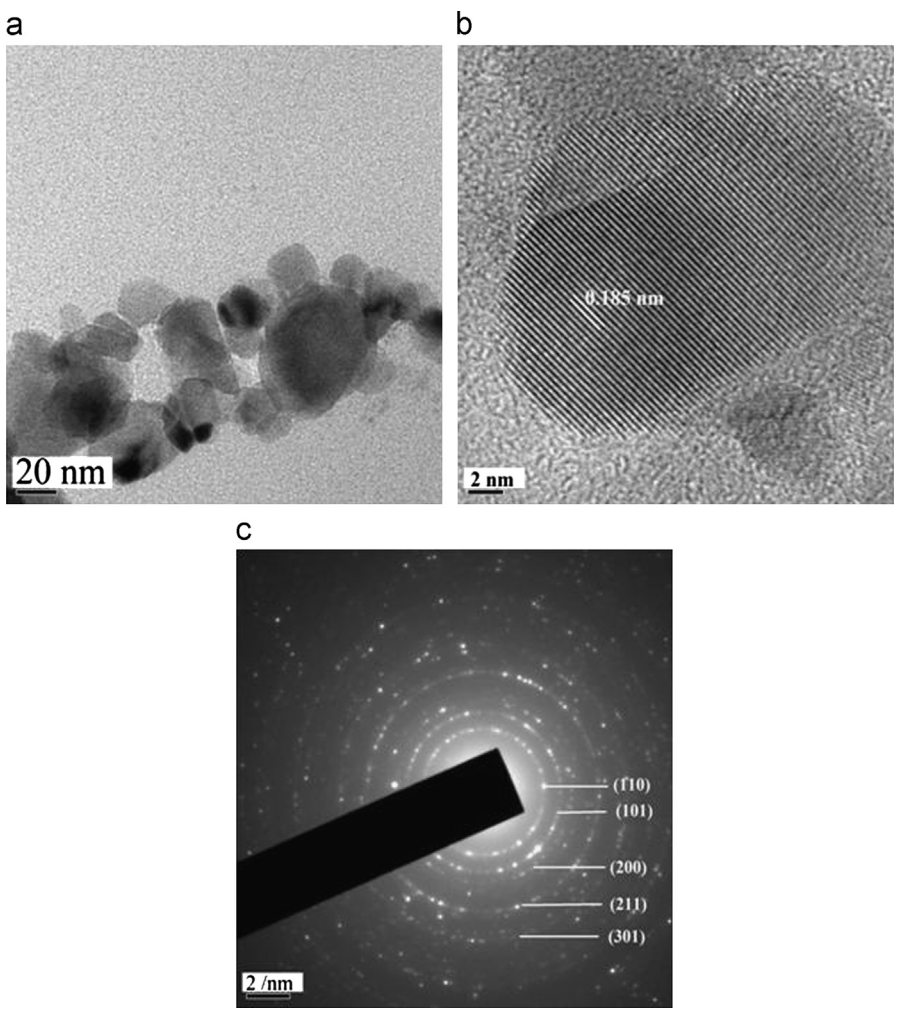

Fig. 2. (a) TEM image of SnO_2 nanoparticles synthesized by the solution combustion method, (b) HRTEM image of a single SnO_2nanocrystal and (c) SAED pattern of single SnO_2nanocrystal.

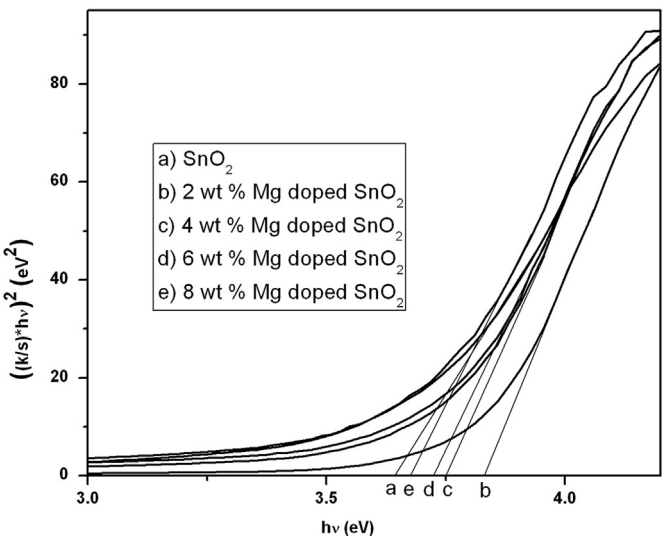

Fig. 4. Tauc plots of SnO_2 and Mg doped SnO_2 synthesized by the solution combustion method.

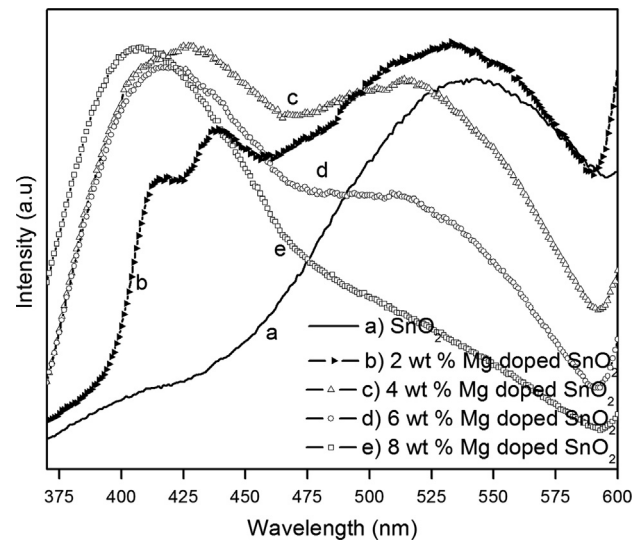

Fig. 5. PL spectra of SnO_2 and Mg doped SnO_2 synthesized by solution combustion method.

decrease the band gap. On the other hand the dopant Mg goes to interstitial site in the host lattice, the concentration of holes may reduce and hence band gap value may decrease. In the present case, while doping with 2 wt% Mg in SnO_2 the Mg atoms probably enter into the interstitial site in SnO_2 lattice. As a result we observed a band gap value of 3.82 eV. However for higher doping concentrations the quantity of substitutional Mg atoms may greater than Mg occupied in the interstitials. Thus band gap of the material likely to reduce as observed in the present case.

3.4. Photoluminescence analysis

The PL emission spectrum of SnO_2 is broad which is extended from 510 to 550 nm and centered at 540 nm (Fig. 5a). Additional weak peaks are observed in 2 wt% Mg doped SnO_2 at 417 and 439 nm. The intensity of peaks at blue region increases and merge together with increase in concentration of Mg^{2+} ion, and the intensity of green emission decreases (Table 2). In the case of 4 wt % Mg doped SnO_2 peaks in the blue region as well in the green region having almost same intensity ($I_b/I_g = 1.05$). Intensity of broad band in the blue region is enhanced and band in the green region having comparatively less intensity in 6 wt% Mg doped SnO_2. It is interesting to note that in 8 wt% Mg doped SnO_2, only blue band is observed. The present optical studies reveals that optical band gap of the as synthesized samples varies from 3.6 to 3.8 eV (345–370 nm) which is shown in Table 2. So the observed PL bands are not merely contributed to direct recombination of conduction electrons and holes in the valance band. Broadening of PL spectra of samples is probably due to different energy states located within the band gap. However the defects and impurities present in crystalline structure contribute to emission in the visible region.

One can see an emission at 540 nm in SnO_2 and is due to the presence of structural defects like tin interstitials. The blue emission appeared at 417 and 439 nm is generated due to the formation of additional defect levels introduced by Mg dopant. Generally, oxygen vacancies are the common defect in nanocrystalline metallic oxides which act as luminescent centers [30,31]. The possible charged states of oxygen vacancies are V_o^0, V_o^+ and V_o^{2+} [10]. Among these V_o^0 is a shallow donor which lies near the conduction band. Most of the oxygen vacancies likely in the V_o^+ state under flat-band conditions, V_o^+ state combine with a hole may generate V_o^{2+} state.

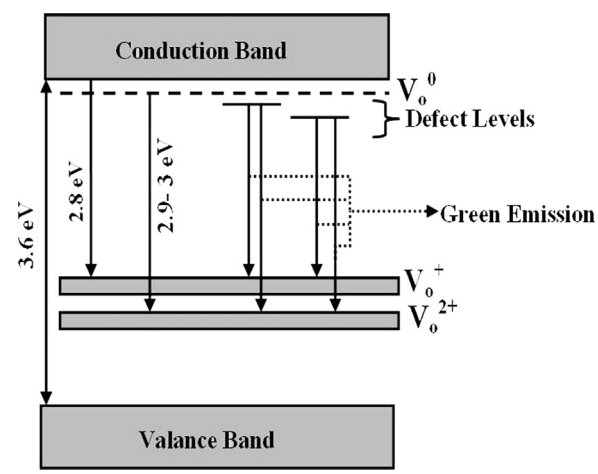

Fig. 6. Schematic representation of relaxation process in photoexcited SnO_2 lattice.

The schematic band diagram of Mg doped SnO_2 nanostructures is given in Fig. 6.

The relaxation process of photoexcited electron in SnO_2 lattice likely to occur in different ways. If the energy of excitation photon is greater than the band gap energy of SnO_2, the electron excited to the conduction band leaving a hole in the valance band. These photo-excited electrons can recombine with V_o^+ or V_o^{2+} center. Even at room temperature V_o^0 level dissociates into V_o^+ level and a conduction electron and vice versa. When an electron de-excite to V_o^+ state, the electron combines with V_o^+ state and consequently V_o° state will be generated, the intensity of V_o^0 state will increase. Thus in effect, the relaxation process is simply the change over state from V_o^+ to V_o^0 state. On the other hand, the probability to occur radiative emission from V_o^+ state is less. The observed weak emission at 440 nm in 2 wt% Mg doped SnO_2 probably due to the above process. Recombination of an excited electron to V_o^{2+} level gives the blue emission observed at lower wavelength. Since ionic radii of Sn^{4+} (0.69 Å) and Mg^{2+} (0.72 Å) are comparable, Mg can easily substitute for Sn^{4+} in host lattice [32]. The deficiency of 2^+ charge can be considered as an oxygen vacancy. In other words, the incorporation of Mg^{2+} into host lattice creates an oxygen vacancy V_o^{2+}. So the intensity at 417 nm is increased with concentration of Mg and is consistent with the obtained optical band gap values.

4. Conclusions

The optical band gap and PL emission nature of SnO_2 is modified due to the Mg incorporation in SnO_2 lattice. A combined blue and green emission observed in 4 wt% Mg doped SnO_2 is attributed to the oxygen vacancies (V_o^{2+}) and tin interstitials. Intensity enhancement corresponds to blue emission with increase in Mg doping concentration is due to the increase in population of oxygen vacancies. Combined blue and green emission property of 4 wt% Mg doped SnO_2can be used for electron injection in heterojunction LEDs in order to generate white light.

Acknowledgments

Shajira P S is thankful to University Grant Commission, New Delhi for awarding Junior Research Fellowship. Authors are thankful to Jayasree RS, Sree Chitra Tirunal Institute for medical sciences and Technology, Biomedical Technology Wing, Thiruvananthapuram for PL measurements and KSCSTE, Government Kerala, India for financial assistance for the work under SRS Scheme (No.081/2012/KSCSTE).

References

[1] E.R. Leite, I.T. Weber, E. Longo, J.A. Varela, Adv. Mater. 12 (2000) 966.
[2] S. Ferrere, A. Zaban, B.A. Gsegg, J. Phys. Chem. B 101 (1997) 4490.
[3] O.A. Ghandour, D. Constantinide, R.E. Sheet, A. Ghandour, Proc. SPIE 4637 (2002) 90.
[4] W. Dazhi, W. Shulin, C. Jun, Z. Suyuan, L. Fangqing, Phys. Rev. B. 49 (1994) 282.
[5] G. Ansari, P. Boroojerdian, S.R. Sainkar, R.N. Karekar, R.C. Aiyer, S.K. Kulkarni, Thin Solid Films 295 (1997) 271.
[6] M. Gaidi, A. Hajjaji, R. Smirani, B. Bessais, M.A. ElKhakani, J. Appl. Phys. 108 (2010) 063537.
[7] T.S. Herng, S.P. Lau, S.F. Yu, S.H. Tsang, K.S. Teng, J.S. Chen, J. Appl. Phys. 104 (2008) 103104.
[8] E.J.H. Lu, C. Ribeiro, T.R. Giraldi, E Longo, E.R. Leite, J.A. Varela, Appl. Phys. Lett. 84 (2004) 1745.
[9] S. Munnix, M. Schmeits, Phys. Rev. B 27 (1983) 7624.
[10] K. Vanheusden, W.L. Warren, C.H. Seager, D.R. Tallant, J.A. Voigt, B.E. Gnade J. Appl. Phys. 79 (1996) 7983.
[11] K.G. Godinho, A. Walsh, G.W. Watson, J. Phys. Chem. C 113 (2009) 439.
[12] M. Zervos, A. Othonos, J. Cryst. Growth 340 (2012) 28.
[13] H.W. Kim, N.H. Kim, J.H. Myung, S.H. Shim, Phys. Status Solidi A 202 (2005) 1758.
[14] J.H. He, T.H. Wu, C.L. Hsin, K.M. Li, L.J. Chen, Y.L. Chueh, L.J. Chou, Z.L. Wang, Small 2 (2006) 116.
[15] F. Gu, S.F. Wang, M.K. Lu, Y.X. Qi, G.J. Zhou, D. Xu, D.R. Yuan, Inorg. Chem. Commun. 6 (2003) 882.
[16] F. Davar, F. Mohandes, M.S. Niasari, Polyhedron 29 (2010) 3132.
[17] E. Elangovan, K. Ramamurthi, J. Optoelectron. Adv. Mater. 5 (2003) 45.
[18] D.F. Zhang, L.D. Sun, J.L. Yin, C.H. Yan, Adv. Mater. 15 (2003) 1022.
[19] R.D. Tarey, T.A. Raju, Thin Solid Films 128 (1985) 181.
[20] V. Schlosser, G. Wind, in: Proceedings of the 8th EC Photovoltaic Solar Energy Conference, Florence, Italy, 1998 p. 998.
[21] D. Wang, S. Wen, J. Chen, S. Zhang, F. Li, Phys. Rev. B 49 (1994) 14282.
[22] P. Chetri, A. Choudhury, Physica E 47 (2013) 257.
[23] L. Fraigi, D.G. Lamas, N.E.W. Reca, Nanostruct. Mater. 11 (1999) 311.
[24] B.D. Cullity, Elements of X-ray Diffraction, Addison-Wesley Publishing Co., USA, 1956.
[25] Z.W. Chen, J.K.L. Lai, C.H. Shek, Phys. Rev. B 70 (2004) 165314.
[26] S. Chacko, M.J. Bushiri, V.K. Vaidyan, J. Phys. D: Appl. Phys 39 (2006) 4540.
[27] P. Kubelka, F. Munk, Z. Tech. Phys. (Leipzig) 12 (1931) 593.
[28] B. Nasr, S.D. Gupta, D. Wang, N. Mechau, R. Kruk, H. Hahn, J. Appl. Phys. 108 (2010) 103721.
[29] P. Wu, B. Zhou, W. Zhou, Appl. Phys. Lett. 100 (2012) 182405.
[30] L.Z. Liu, X.L. Wu, J.Q. Xu, T.H. Li, J.C. Shen, P.K. Chu, Appl. Phys. Lett. 100 (2012) 121903.
[31] L.Z. Liu, J.Q. Xu, X.L. Wu, T.H. Li, J.C. Shen, P.K. Chu, Appl. Phys. Lett. 102 (2013) 031916.
[32] M.J. Weber, Handbook of Optical Materials, CRC Press, Boca Rota, USA, 2003.